Simulation of plasma confinement in an electron cyclotron resonance zero-B trap

Simulación de un plasma calentado mediante resonancia ciclotrónica electrónica confinado en una trampa magnética cero-B

Valeriy Dondokovich Dugar-Zhabon
Ph.D. Physics. Universidad Industrial de Santander
Bucaramanga, Colombia
vdougar@uis.edu.co

Anatoly Umnov
Ph.D. Physics, University of Russia
Moscow, Russia
anumnov@yandex.ru

Mao Tsetung Murillo-Acevedo
Ph. D(c) Physics. Universidad Santo Tomas
Bucaramanga, Colombia
maotsetungmurillo@mail.ustabuca.edu.co

Resumen– **Actualmente el estudio del comportamiento de plasmas en campos magnetostáticos asimétricos de configuración compleja solo es posible a través de simulación computacional. La eficiencia de confinamiento del plasma en una trampa cero-B, el cual es comprimido longitudinalmente por un espejo magnético y transversalmente por el campo de un hexapolo magnético, es determinada a través del método de partícula en celda electrostático. En el modelo simulado el plasma es calentado por microondas de 14 GH cuya potencia es transmitida a los electrones mediante resonancia ciclotrónica. La distribución espacial de la componete iónica y electrónica es mostrada. Se encuentra que la población electrónica puede ser dividida en tres grupos, fríos, calientes y super calientes. Los datos obtenidos para la distribución de la densidad tanto radial como longitudinal son comparados con las mismas distribuciones encontradas para la trampa mínimo-B. Como resultado se encuentra que la trampa cero-B presenta algunas ventajas frente a la trampa mínimo-B.**

Palabras clave– **Trampa magnética, resonancia ciclotrónica electrónica, simulación mediante el método partícula en celda.**

Abstract– **Currently the study of the nonlinear plasma evolution in magnetostatic fields of complex asymmetrical configurations is possible only through computer simulations. The confinement efficiency of plasma by a magnetic zero-B trap which is comprised of longitudinal mirror and transversal hexapole cusp fields is determined through a particle-in-cell method in the electrostatic approximation. In the simulation model the plasma heating by 14 GHz microwave power is realized at electron cyclotron resonance conditions. The space localizations of electron and ion components are visualized. It is found that the plasma electron population can be subdivides into cold, hot and superhot groups. The obtained data for the ion density distribution along radial and longitudinal trap directions are compared with the same distributions calculated for the case of minimum-B trap. It is found that the zero-B trap has some advantage over the minimum-B trap in reference to the Lawson criterion.**

Keywords– **magnetic trap, electron cyclotron resonance, particle-in-cell simulation.**

1. INTRODUCTION

It is well known that the minimum-B trap supplemented with microwave field at electron cyclotron resonance (ECR) conditions is generally used as a base for multicharged ion source designing because the minimum-B space configuration guarantees the MHD stability of the confined plasma and the microwave power at ECR heats the electrons to energies necessary to eject an inner atomic electron. In the last few decades, many experimental efforts have been made to adapt the minimum-B geometry to a number of practical applications, each requiring specific parameters for the corresponding objectives [1]. A phenomenological study and a three-dimensional (3D) plasma simulation in a minimum-B trap [2-5] show that the space plasma structure is determined by the magnetic field pattern and the ECR surface space shape. Furthermore, the experimental data on existence of cold, hot and superhot electron

groups are explained through the corresponding theoretical constructions. The hot electrons very likely gain their energies due to collective plasma-wave interactions in the cyclotron and high-hybrid resonance conditions [6]. A mechanism of electron heating to energies of hundreds kilo-electron-volts is attributed to the space cyclotron autoresonance electron-microwaves interaction [7, 8]. Recently this autoresonance interaction has helped to understand how electron rings, which are experimentally observed in the magnetic mirror traps [9-11], are self-organized [12]. In this paper, we report the most recent 3D simulation results on plasma confinement in the ECR zero-B trap formed by two cusp magnetic systems which was proposed in [13].

2. THE ECR TRAP SETUP

In the conventional ECR minimum-B traps, the magnetic field is generated by a radial multicusp system and axially symmetrical current coils where the direct currents run in the same direction. The cusp field is generated by the permanent magnetic bars equally spaced on the discharge chamber cylindrical surface, namely along its axis that coincides with the coil axis. The magnetic field in the minimum-B trap increases when going from the minimum field point in all the directions, giving MHD stability to the plasma, and thus inhibiting the dangerous flute instability [14]. The confined plasma is heated by microwaves on the magnetic surface where ECR conditions are fulfilled. To produce a smooth ECR surface, usually of a near-ellipsoidal shape, the cusp bar pair number must be as greater as possible while the space limited for their accommodation on the discharge chamber surface results in turning the hexapole and octpole bar systems to practical use [1].

The principle schemes of the zero-B and minimum-B traps are identical differing only in the current directions; the currents in the zero-B coils flow in the opposite directions [13]. The magnetic field of the studied zero-B trap is composed of a hexapole cusp system and two cusp coils. The hexapole cusp field, produced by six bars of 2.5 cm wide by 3 cm high and 20 cm long which are arranged on the outer surface of the cylindrical chamber of 6.4 cm in diameter and 24 cm in length, is calculated by the method of equivalent solenoids on the assumption that the field on the bar surfaces is to be equal to 1.2 T. All the magnetic elements which comprise the zero-B trap are identical to those of the minimum-B trap described in [5] in order to make it possible to confront the simulation results obtained for these traps. 3D image of the zero-B magnetic lines is very complex; however their vector projection picture on a longitudinal cross section is rather simple. Figures 1 and 2 give the magnetic field vectors on the plane which passes through the centerlines of the opposite magnetic bars (an *xz* - plane with the trap axis as the z-axes) for the minimum-B trap and the zero-B trap respectively. The vector line distributions evidence that both of these trap fields doesn't possess the symmetry properties; the zero-B field is in a greater extent. The complete vector picture in the plane which passes between the bars cannot be demonstrated appropriately because of azimuth magnetic field component. Figure 3 shows the longitudinal magnetic field profiles for both traps in the (r=0, z)-plane which passes through the opposite bar centerlines. The currents in the coils are adjusted in such a manner that the peaks on the longitudinal magnetic profiles should be of the same magnitude and should be located at the same distance of 9.2 cm on both sides of the both traps centers (see Fig. 3). This adjustment of currents and the peak positions result in the plasma parameters calculated for the present minimum-B trap somewhat different from the data depicted in [5].

In the median transverse plane, the minimum-B magnetic field profile along the radius directed to the centre of one of the bars is shown as the dash curve 3 in Fig.4. Contrary to the minimum-B trap, where the coil field does not contribute to the radial magnetic component in this plane, in the zero-B trap the coil field strengthens the radial magnetic tension in the points which lie on the radius directed to the center of any hexapole bars (the curve 1, Fig.4) and weakens the magnetic field along the radius line that passes between the neighboring bars (the curve 2, Fig.4). For the zero-B trap, the total magnetic field increases in the vicinity of one of the hexapoles and decreases at diametrically opposed points due to the coils field (see Fig.2). The minimum-B magnetic field curves presented in Fig.4 are somewhat different from those shown in [5] because, as has been mentioned above, the minimum-B and zero-B coil currents are adjusted to equalize the magnitude of the magnetic field peaks and their positions.

Fig.1. MINIMUM-B TRAP VECTOR FIELD PICTURE IN THE LONGITUDINAL PLANE PASSING THROUGH THE OPPOSITE BAR CENTERLINES

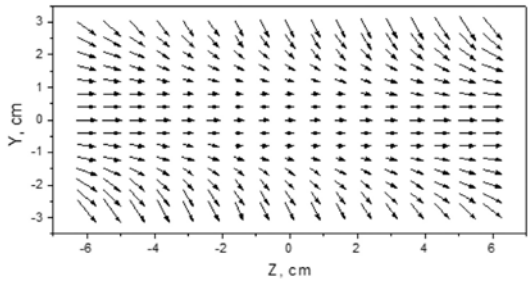

Source: the authors.

Fig.2. ZERO-B VECTOR MAGNETIC FIELD PICTURE IN THE LONGITUDINAL PLANE PASSING THROUGH THE OPPOSITE BAR CENTERLINES

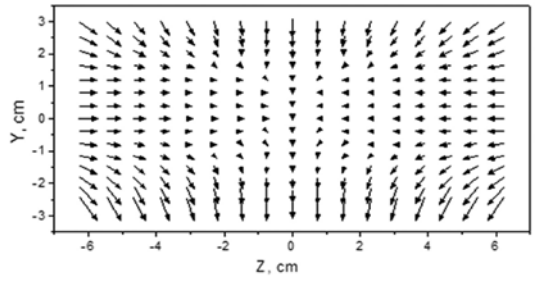

Source: the authors.

The electrons are predominantly heated when they pass through the ECR surface $B_0\left(\vec{r}\right)=mc\,\omega/e, where\ \omega, e,$ and c are the electromagnetic field frequency, the charge and mass of electron and the light speed respectively. The chosen microwave frequency of 14 GHz is commonly used for ECR ion source functioning [1]. The 3D surface where the electrons meet the cyclotron resonance is determined by the equation $B_0\left(\vec{r}\right)=5$ kGs. A longitudinal section of the zero-B ECR surface has a near-elliptical shape with a long semi-axis of 4.3 cm (Fig.3). In the transverse median plane, the ECR surface radius varies from 1.9 cm to 2.3 cm as shown in Fig.4. It should be mentioned that the ECR ellipsoid is actually an ellipsoid-like layer of the finite thickness because the electron mass depends on its energy. For the used microwave field, the cutoff plasma density, which is proportional to the square of the microwave frequency, is 2.36 x 10^{12} cm^{-3}. A multimode regime for the electromagnetic field in the chamber is assumed because the wavelength is at least 3 times smaller than the discharge chamber dimensions and of the density inhomogeneous plasma presence. Because of this, the microwave electric field vectors are suggested to be distributed in the chamber volume randomly. The microwave electric field is taken equal to 0.5 kV/cm.

A physical difference between the minimum-B and the zero-B type traps is significant although there is no difference in their designs. From Figs.3 and 4, where the longitudinal and radial profiles of the magnetic fields for both traps are traced, one can see that they cannot be compared in terms of the mirror ratio which has a finite value for the minimum-B trap and is infinite for the zero-B trap. Because of this, the loss cone concept is unsuitable for the zero-B trap. It is important for plasma confinement efficiency that the core volume, limited by the closed ECR surface, is larger in the zero-B trap as compared with the minimum-B trap; in our case by a factor of 2.3, to be more exact.

Fig.3. LONGITUDINAL MAGNETIC FIELD PROFILES IN THE PLANE PASSING THROUGH THE OPPOSITE BAR CENTERLINES FOR THE MINIMUM-B TRAP AND ZERO-B TRAP

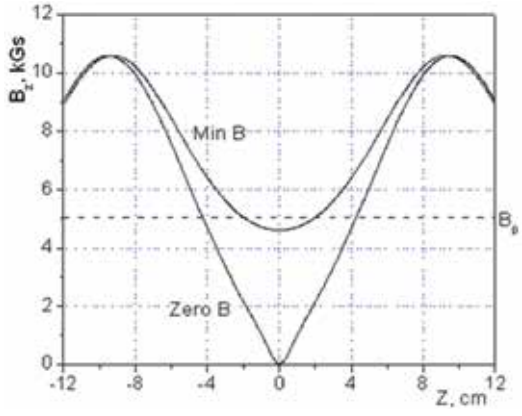

Source: the authors.

Fig.4. RADIAL MAGNETIC FIELD PROFILES ALONG THE DIRECTION TO: 1 – THE CENTRE OF A ZERO-B TRAP BAR, 2 – A POINT LOCATED BETWEEN NEIGHBORING ZERO-B TRAP BARS, 3 - THE CENTRE OF A MINIMUM-B TRAP BAR

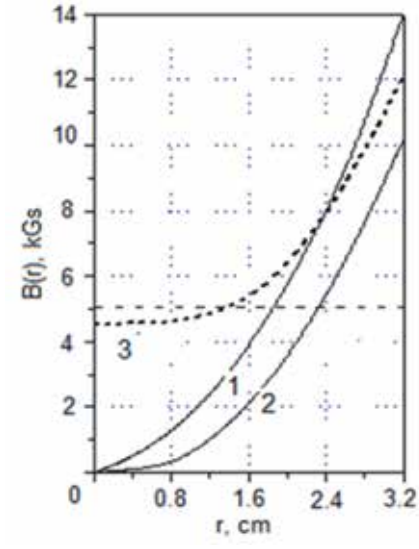

Source: the authors.

3. SIMULATION

In order to study the zero-B confinement efficiency and save the computer time, the fully ionized plasma of the lightest gas is simulated. Initially, the cavity is filled uniformly with $6x10^{13}$

charge particles which are the electrons and protons. The chamber walls are treated as absorbing but in order to conserve the total number of particles and arrive to the stationary state; the absorbed particles are substituted for identical ones that are distributed at random in the total plasma volume. The calculation process is considered to be completed when the plasma comes to the dynamic steady-state in which the plasma topology and particle energy distribution experience only small fluctuations. The steady-state plasma parameters obtained for the both of the studied traps are compared.

For the ECR simulations, the initial particle energies must be small with respect to the energies of the final steady-state which is determined by the microwave field parameters and the magnetic field configuration. As we shall see later, the steady-state energies of the electrons are in the kilo-electron-volt band and the ions have the energies of the order of tens and hundreds electron-volts. This explains why the initial electron and ion energies of 5 eV and 0.5 eV, respectively, are considered appropriate. For the simulations, the discharge chamber volume is divided into 3D discrete cells that form a uniform 32x32x64 volume mesh. For the simulations, a very short time step $\Delta\tau$ of the $4x10^{-3}$ fraction of the microwave period is chosen. Such a small time step together with the modest mesh spacing makes the simulation of the cyclotron resonance interaction correct and permits to avoid the progression of dangerous spurious numerical modes. Second, the number of superparticles in a cell must be vastly more than one superparticle for each species [14, 15].

The particles which reach the cavity walls are considered lost, but in order to conserve the total number of particles and plasma neutrality, they are replaced by identical particles which are introduced into the plasma volume at random points. This computer procedure simulates the constant injection of plasma particles into the real magnetic traps or neutral atom ionization in the chamber like it occurs in the negative ion sources.

In this paper, an explicit particle-in-cell (PIC) method is applied to the numerical solution of the motion equation which is well matched to the plasma characteristics determination [15, 16]. For a multiparticle system computing it is important that the PIC methods filtering out the short range interaction between the individual particles are numerically less diffusive when compared to the other simulation techniques that presume high calculation accuracy [17, 18]. The PIC method requires that all particles of a small phase space element are described by one computational particle or superparticle. The coordinate superparticle image is not of the classical particle but represents a finite-sized cloud of electrons and ions which remain in the cloud at each simulation time step *n*. The cloud shape function is taken cubic, with the dimensions equal to the cell sizes. The difference between the electron and the ion mobilities results in generating the self-consistent electrostatic field which changes at each time step. The self-consistent electrical potential Φ in the mesh nodes are submitted to the Poisson equation which in a finite-difference form is

$$\frac{\Phi^n_{i+1\,jk}-2\Phi^n_{ijk}+\Phi^n_{ij-1k}}{\Delta x^2}+\frac{\Phi^n_{ij+1k}-2\Phi^n_{ijk}+\Phi^n_{ij-1k}}{\Delta y^2}+\frac{\Phi^n_{ijk+1k}-2\Phi^n_{ijk}+\Phi^n_{ijk-1}}{\Delta z^2}=-4\pi\rho^n_{ijk}\quad(1)$$

where Φ and ρ are normalized to $\Phi_0=B_0 c r_L$ and $\rho_0=B_0 c/r_L$ respectively, and the coordinates (*x, y, z*) are given in units of the relativistic Larmor radius $r_L=c/\omega$. The charge density ρ_{ijk} in the mesh nodes is determined through a volume-weighting assignment scheme for the simulation suiperparticles. Because the computational mesh is periodical, the fast Fourier transform (FFT) method is accepted for Poisson equation solving [18]. The FFT method permits to replace eq. (1) by the equations for the Fourie amplitudes and resolve them for the mesh nodes. Beginning with the calculated amplitudes, the mesh node electric potentials determine the self-consistent electric field E^{sn}_{ijk} through the finite-difference derivatives:

$$\left(g^{sn}_{ijk}\right)_x=\frac{\Phi^n\left(i-1,j,k\right)-\Phi^n\left(i-1,j,k\right)}{2\Delta_x}\quad(2)$$

where $g_{ijk}^{sn} = eE_{ijk}^{sn} / (mc\omega)$. The other field components are found in the same manner. The self-consistent field $\vec{g}^{sn}(x,y,z)$ in the cloud center mass is found out beginning with the node values through the bilinear interpolation scheme generalized for 3D case.

The time evolution of the electron and ion motions are described by the Newton-Lorentz equation which in a finite difference dimensionless form is

$$\frac{\vec{u}^{n+1/2} - \vec{u}^{n-1/2}}{\Delta} = \vec{g}^{n} + \frac{\vec{u}^{n+1/2} - \vec{u}^{n-1/2}}{2\gamma^{n}} \times \vec{b}^{n} \quad (3)$$

where $\vec{u}$ is the particle momentum in units m_0c^2, $\vec{g}^{n} = \vec{g}^{sn} + \vec{g}^{wn}$ of represents the total electric field, is the normalized microwave electric field, $\Delta\tau = \omega\Delta t$ stands for the simulation time step and $\gamma = (1+u^2)^{1/2}$ is the relativistic factor.

Equation (3) for the electrons is considered relativistic not only because the electrons can acquire a high energy in the resonance conditions but also due to the exceptional sensitivity of the ECR interaction to phase the difference between the electric field and the particle velocity. As for the ions, they cannot participate in interaction with the microwaves in any point of the trap, which permits to treat eq. (3) for them as non-relativistic. The calculation programs applied in this work are exactly the same which are used in [13] for the computer simulation of an ECR minimum-B trap plasma. Equation (3) is integrated by using the second order explicit Boris leapfrog technique which is very efficient for many particle problems [16]. To start the leapfrog-scheme, the velocity for the moment $\tau = 0$ and the initial coordinates for the moment $\tau = \Delta\tau/2$ as well as the electric field values are specified. The problem solution procedure is the self-consistent since eqs. (1) and (3) are in association and must be solved simultaneously at each time step. Thus, the problem to be solved is the motion of electrons and ions in applied magnetic and microwave fields and their own electric field.

4. RESULTS AND DISCUSSIONS

For simulations, the total number of the real particles is divided into 4.2x10^5 superparticles with the charge-to-mass ratio identical to the real particles. The chosen amount of the superparticles guarantees that at least 10 of them reside in the core zone cells. The elaborated algorithm permits to visualize the plasma space configuration and the energy distribution function at every time step as well as the plasma space shape. The simulations show that the principle parameters, like the space plasma distribution and the electron energy distribution function, come to a steady-state after 1x10^6 time steps for the minimum-B trap and after 5x10^6 time steps for the zero-B trap. In the steady state, the longitudinal and radial ion density distributions, shown in Figs.5 and 6, clearly demonstrate that the plasma density in the core zone of the zero-B trap (the solid curves) is approximately 1.3 times greater than in the minimum-B case (the dashed curves). In the corona zone, outside the ECR surface, both trap densities do not differ very much.

Fig.5. LONGITUDINAL ION DENSITY DISTRIBUTIONS FOR THE MINIMUM-B TRAP (CURVE 1) AND THE ZERO-B TRAP (CURVE 2)

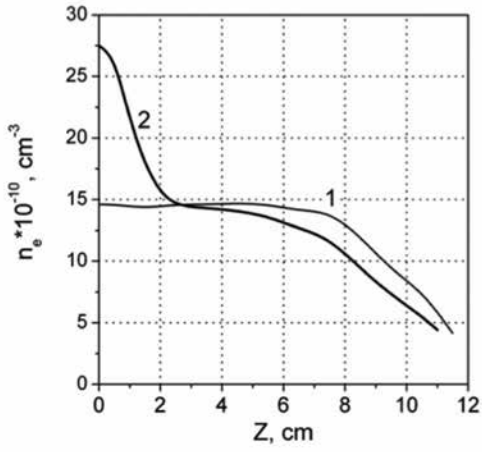

Source: the authors.

Fig.6. RADIAL ION DENSITY DISTRIBUTIONS FOR THE MINIMUM-B TRAP (CURVE 1) AND THE ZERO-B TRAP (CURVE 2)

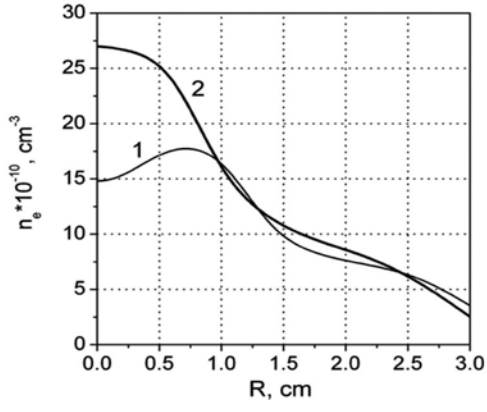

Source: the authors.

The ion density distributions for both traps principally coincide with the electron ones (see Figs. 5 and 6). The elevated density in the centre of the both traps is directly related to the ECR interaction: the electrons which are accelerated in the vicinity of the closed ECR surface acquire large magnetic moments and consequently are pushed by the diamagnetic force to the trap centers; the higher magnetic gradient in the zero-B trap caused better plasma confinement efficiency. A larger core volume and higher core plasma density in the zero-B trap result in that the total number of ions captured inside the ECR surface for the zero-B trap is 3.7 times higher than for the minimum-B trap.

Figures 7 and 8 show the pictorial renditions of ion and electron component localizations in the zero-B longitudinal plane layer of 0.2 cm thick. In these figures the transverse axis scale is enlarged in order some structure details to be elucidated. These space distributions evidence that the plasma run into some problems with crossing the transverse median plane of the zero-B trap; such difficulties do not occur in the minimum-B trap. Outside the core zone, the ions are located predominantly along the chamber axis forming something like a cylinder of 0.6-0.8 cm in diameter. Such geometry of the ion space distribution suggests that the density of the ion flux which incidents on the center of a chamber end-wall is significantly higher than the density of the ion fluxes which fall on any other part of the inner wall surface. In this regard the zero-B trap looks like the minimum-B trap. Figure 9, where the ion component distribution in the median transversal layer of 0.2 cm in thick is demonstrated, shows that the ion population fits the hexapole magnetic structure as observed in the minimum-B case [5].

Fig.7. LOCALIZATION OF THE IONS IN A LONGITUDINAL CENTRAL LAYER OF 0.2 CM THICK FOR ZERO-B TRAP

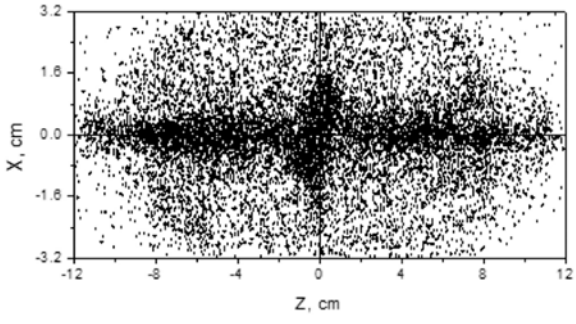

Source: the authors.

Fig. 8. LOCALIZATION OF THE ELECTRONS IN A LONGITUDINAL CENTRAL LAYER OF 0.2 CM THICK FOR ZERO-B TRAP

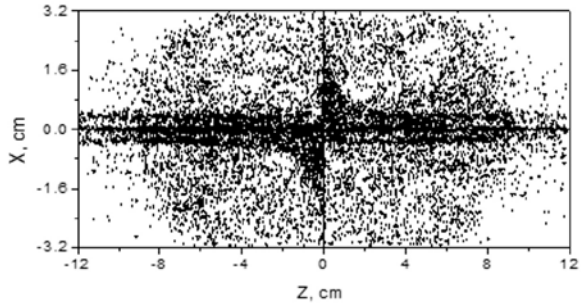

Source: the authors.

Fig.9. LOCALIZATION OF THE IONS IN THE MIDDLE TRANSVERSE CROSS LAYER OF THE 0.2 CM THICK FOR ZERO-B TRAP

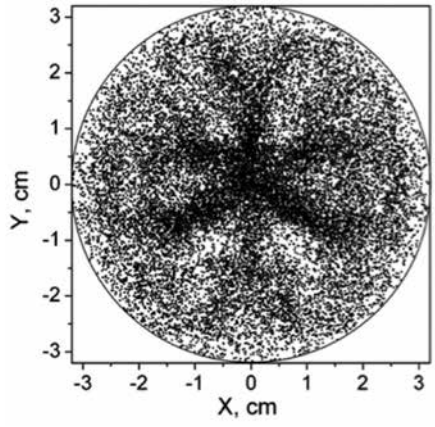

Source: the authors.

Fig.10. ELECTRON ENERGY DISTRIBUTION IN THE SEMI-LOGARITHMIC SCALE: 1 – COLD ELECTRONS, 2 – HOT ELECTRONS

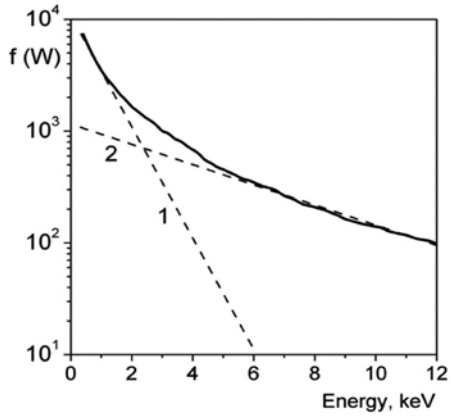

Source: the authors.

The coexistence of distinct electron groups, each being determined by its proper effective temperature is a specific property of the ECR plasmas. The electron energy spectrum of two zero-B groups is displayed in a semi-logarithm scale in Fig. 10. The bulk electrons whose effective temperature is of 1.9 keV overwhelm the electron majority in

the corona region which is spaced outside the ECR surface layer. The hot electrons characterized by effective temperature of 6 keV are predominately found captured in the core zone limited by the ECR surface. For the core zones, the relative number of electrons with energies over 1 keV has proved to be smaller for the zero-B trap than for the minimum-B trap (see Fig.11). The significant difference in the areas under these curves is accounted for the fact that in the ECR zero-B core zone are found confined vastly more particles than in the ECR minimum-B core zone.

For the zero-B trap some improvement in the electron heating efficiency can be achieved by decreasing the magnetic gradient in the ECR zones. It is found also the superhot fraction with energies higher than 50 keV. The population of this fraction is very small, of the order of 0.01% of all the electrons. Its particular influence on the plasma behaviour is not established.

Fig.11. ELECTRON ENERGY DISTRIBUTIONS IN THE CORE ZONE FOR: 1 - MINIMUM-B TRAP 2 - ZERO-B TRAP

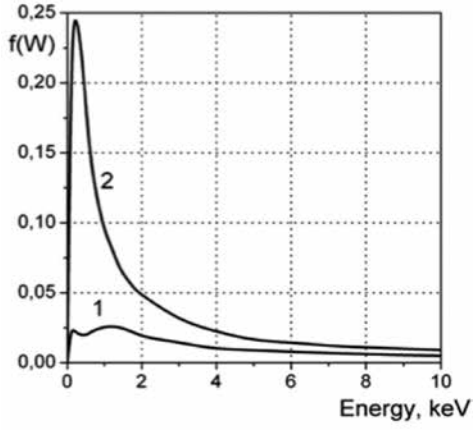

Source: the authors.

Fig.12. ENERGY DISTRIBUTION OF THE IONS CONFINED IN THE CORE ZONE

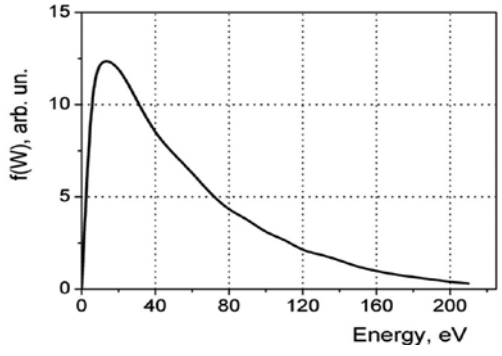

Source: the authors.

The ions gain their energies in the self-consistent electric field which manifests itself as fast chaotic local potential fluctuations. The energy distribution of the ions in the core zone is extended approximately to 200 eV at the most probable ion energy is of 20 eV (see Fig. 12).

The plasma lifetime for both traps is evaluated in the regime of freely decaying plasma, i.e. without substitution of the particles lost on the chamber walls by others. Figure 13 presents the time decaying curve of the total particle number in the zero-B trap. This curve which is given in a semi-logarithm scale can be divided into three time-intervals. The strong drop during the first 5 μs owes to abrupt cessation of substitution of the particles lost on the absorbing walls. The second interval of (10-75) μs can be associated with the corona plasma decaying with the characteristic decay-time of 26 μs. The slow decrease of the particle number observed after a lapse of 150 μs is determined by the large plasma lifetime in the core zone which is estimated at 1.6 ms. The plasma decay-curve for the ECR minimum-B trap is not presented because on the scale of Fig.13 it practically coincides with the curve for zero-B trap, but the characteristic times are slightly different. For the minimum-B trap, the corona lifetime is 30 μs and the calculated core lifetime is 1.4 ms. Confinement efficiencies of the ECR traps can be compared through the Lowson criterion $n\tau$ for the core plasma. The confinement efficiency of the zero-B trap is found higher than that of the minimum-B trap: $(n\tau)_{\text{zero-B}} / (n\tau)_{\text{min-B}} \cong 1.3$. It is appropriate at this point to recall that the core zone volume is significantly larger for the zero-B trap as compared with the minimum-B trap.

Fig.13. PLASMA DECAY-CURVE FOR THE ZERO-B TRAP

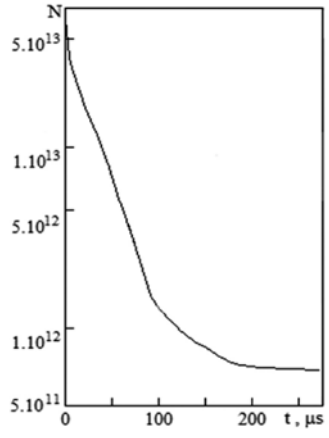

Source: the authors.

5. CONCLUSIONS

A novel type of ECR plasma magnetic trap consisting of a longitudinal cusp and multipole transversal cusp systems is proposed. The specific features of this zero-B trap are zero magnetic field value in the center of the trap and a non-symmetrical space field configuration. With a theoretical analytical study of the plasma behavior being unpractical, we examine the efficiency a zero-B trap through PIC/Poisson computer simulation. A comparison of the calculated Lowson criteria for the zero-B trap and the minimum-B trap evidences that the zero-B trap offers a larger efficiency in respect to the plasma confinement. In the upcoming zero-B trap numerical study, the hydrogen plasma will be changed for the argon plasma and the ionization processes will be incorporated into the computer code. Such changes allow to meet the multicharge ion production rates and to calculate the composition and emittance of the extracted ion beams. We are also planning to simulate the process of filling the discharge chamber with a steady cold plasma flow.

REFERENCES

[1] R. Geller, *"Electron Cyclotron Resonance Ion Sources and ECR Plasmas"* Inst. Phys. Publishing, Bristol-Philadelphia, 1994.

[2] V. D. Dougar-Jabon, A.M. Umnov and V.B Kutner, "Calculating method for confinement time and charge distribution of ions in electron cyclotron resonance sources", *Rev Sci Instrum*, vol. 67, p. 1152, 1996.

[3] V. D. Dougar-Jabon, A.J. Chacon Velasco, A.M. Umnov and V.I. Kariaka, "Confinement of Ions in Sources Based on Electron Cyclotron Resonance Phenomenon" *Phys Scripta,* vol. 60, p. 250, 1999.

[4] V. D. Dougar-Jabon, A. M. Umnov, and D. Suescun Diaz, "Three dimensional simulation of an ECR plasma in a minimum-B trap" *Rev Sci Instrum,* vol. 73, p. 629, 2002.

[5] V. D. Dougar-Jabon, A. M. Umnov, and D. Suescun Diaz, "Properties of Plasma in an ECR Minimum-*B* Trap via Numerical Modeling" *Physica Scripta*, vol. 70, no. 1, p. 38, 2004.

[6] K. S. Golovanivsky, V. D. Dougar-Jabon and D. V. Reznikov, *Phys Rev E,* vol. 52, p. 2969, 1995.

[7] V. Dougar-Jabon and E. Orozco, "Cyclotron spatial autoresonance acceleration model", *Phys Rev ST Accel Beams,* 12, 041301, 2009.

[8] V. Dougar-Jabon and E. Orozco, "Three-Dimensional Particle-In-Cell Simulation of Spatial Autoresonance Electron-Beam Motion", *IEEE Trans Plasma Sci* 38, p. 2980, 2010.

[9] H. Ikegami, M. Ikezi, S. Tanaka and K. Takayama, "Shell structure of a hot-electron plasma", *Phys Rev Lett.* vol. 19, p. 778, 1967.

[10] M. Porcolab, L. Friedland and I. B. Bertnstein, "Electron cyclotron resonance heating of plasmas in tandem mirror traps", *Nucl Fusion* vol. 21, p. 1643, 1981.

[11] V. D. Dugar-Zhabon, K. S. Golovanivsky and S. A. Safonov, "An ECR source of multicharged ions HELIOS-12", *Nucl Instrum Meth Phys Res,* vol. 219, p. 263, 1984.

[12] V. D. Dougar-Jabon and M. T. Murillo, "Formation of a hot electron ring in an ECR mirror trap through a particle-in-cell simulation study", *IEEE Trans Plasma Sci,* vol. 38, p. 3449, 2010.

[13] V. D. Dougar-Jabon, F. A. Vivas Mejía and A. M. Umnov, "Plasma confinement in a electron cyclotron double cusp trap", *Phys Scripta* vol. 62, p.183, 2000.

[14] F. Chen, "*Introduction to Plasma Physics"*, p.190, Plenum Press, New York and London, 1974.

[15] R. W. Hockney and J. W. Easwood, *Computer Simulation Using Particles,* McGraw-Hill, New York, 1981.

[16] C. K. Birdsall, and A. B. Langdon, *Plasma Physics via Computer Simulation*, A. Higler Series on Plasma Physics, 1995.

[17] G. Lapenta, F. Inoya, and J. U. Brackbill, "Particle in cell simulation of glow discharges in complex geometries", *IEEE Trans. Plasma Sci*. vol. 23, p. 769, 1995.

[18] E. N. Nikolaev, R. M. Heeren, A. M. Popov, A. V. Pozdneev and K. S. Chingin "Realistic modeling of ion cloud motion in a Fourier transform ion cyclotron resonance cell by use of a particle-in-cell approach", *Rapid Communications in Mass Spectrometry* vol. 21, Issue 22, pp. 3527-3546, november, 2007.